Irregular Subharmonic Cluster Patterns in an Autonomous Photoelectrochemical Oscillator

Iljana Miethe, Vladimir García-Morales, and Katharina Krischer*

Physik-Department E19, Technische Universität München, James-Franck-Strasse 1, D-85748 Garching, Germany

(Received 14 February 2009; published 14 May 2009)

Unusual subharmonic cluster patterns are observed during the oscillatory electro-oxidation of *n*-Si(111) under illumination. 2D *in situ* imaging of the electrode by means of an ellipsometric setup allows local variations in the oxide layer thickness to be monitored. The local oscillators exhibit an irregular distribution of the amplitude with the extrema locked to the constant base frequency of the total current. In addition, Ising 2-phase clustering occurs at half the base frequency. This *intrinsic* dynamics is described by means of a modified complex Ginzburg-Landau equation.

DOI: 10.1103/PhysRevLett.102.194101 PACS numbers: 05.45.−a, 47.54.−r, 82.40.Bj

Pattern formation in spatially extended chemical [1] and electrochemical [2] oscillators has been an active area of research in the last two decades. A wide variety of dynamical behaviors absent in individual oscillators arise as a consequence of their mutual coupling and range from complete incoherence to full synchronization of the local oscillators. The introduction of an external parametric forcing [3] or global coupling [4] enriches significantly the dynamical scenario leading, for example, to a locking of the oscillators to multiples of a base, natural frequency. Depending on the forcing or feedback strength different kinds of cluster patterns were observed.

The electro-oxidation of *n*-Si(111) under illumination is known to exhibit oscillations [5]. So far it has been studied *in situ* mainly with space averaging methods looking at the temporal dynamics with a variety of electrochemical and surface sensitive techniques [6]. Despite some previous tantalizing results, spatiotemporal pattern formation at the semiconductor-electrolyte interface is essentially unexplored because satisfactory resolution of the dynamics both in space and time was never achieved experimentally, precluding further insight.

In this Letter, we present *in situ* measurements monitoring the rich spatiotemporal dynamics at the Si-electrolyte interface. Using contrast enhanced optical microscopy [7], we obtain *in situ* 2D images of the thickness of an oxide layer that forms at the interface during the electrodissolution. A surprising experimental observation is the finding of an unusual clustering and entrainment behavior which is *intrinsic* to the dynamics of the system. We elucidate the observed behavior by means of a modified complex Ginzburg-Landau equation including terms describing a 1:1 resonance and a nonlinear global coupling, whose likely physical origins are a global constraint on the total current flowing through the system and an external Ohmic resistor.

Applying a positive voltage to a Si electrode immersed in a F^- containing electrolyte, two competing reactions take place, the electrochemical oxidation of Si, $Si + 4OH^- + \lambda h^+ \rightarrow SiO_2 + 2H_2O + (4 - \lambda)e^-$, and chemical etching of SiO_2 by F^- ions, $SiO_2 + 6HF \rightarrow H_2SiF_6 + 2H_2O$ [8]. Consequently, the interfacial oxide layer thickness is determined by the relative rates of the two reactions; the interplay of these reactions is also decisive for the occurrence of the oscillatory instability at sufficiently positive potentials. The oxidation reaction proceeds at an appreciable rate, only when sufficient holes are present, necessitating the illumination of *n*-Si electrodes.

Our experimental setup is shown in Fig. 1. The *n*-Si (111) (1–2 Ω cm) working electrode (WE) was positioned vertically in the middle of the cell and illuminated homogeneously with 1.2 mW/cm^2 at 0° incident angle with a red light emitting diode (HighLED Linos, typical wavelength 630 nm). The temporal variations of the spatial distribution of the oxide thickness on the silicon were monitored with an *in situ* ellipsomicroscopic setup [7] adapted to our system: Blue light (HighLED, typical wavelength 470 nm) is elliptically polarized and hits the Si electrode at 70° incident angle. The reflected light is passed through a lens imaging the electrode to an analog camera (JAI CV-A50) and an analyzer (Glan Thompson

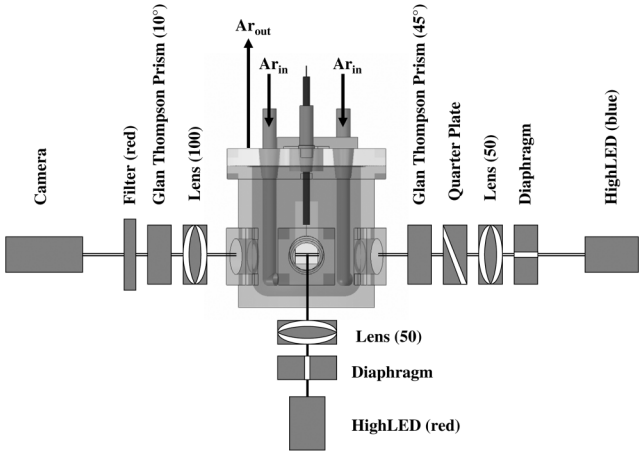

FIG. 1. Scheme of the electrochemical cell and the optical setup used for illumination and ellipsomicroscopic imaging (see text).

prism) converting differences in the polarization state of the (locally) reflected light to intensity differences. A filter is used to keep out scattered red light. The camera images are digitized with a frame grabber (PCI-1405, National Instruments). The electrode had a size of 4.3 mm (x direction) times 2.1 mm (y direction) and was recorded with a resolution of 25 μm in x and 10 μm in y direction limited by the number of pixels of the CCD. The electrolyte was an Ar purged, i.e., oxygen free, 0.5 M NH_4F solution in a three electrode Teflon cell. Counter electrode and reference electrode were a Pt wire bent to a ring and a saturated $Hg|Hg_2SO_4$ electrode, respectively. The potential of the WE was controlled with a FHI-2740 potentiostat (electronic laboratory of the Fritz-Haber-Institut, Berlin, Germany) and, together with the current, digitized with a data acquisition board (PCI-6221, National Instruments). Before immersing into the electrolyte, the Si wafer was cleaned with acetone, ethanol and concentrated NH_4F, rinsed with H_2O and dried with Ar. After purging O_2 from the solution, the open circuit potential is 0.22 V (all voltages are given with respect to the normal hydrogen electrode). A 30 kΩ Ohmic resistor was placed between the WE and the potentiostat, and during the experiments the solution was stirred with a magnetic stirrer.

At intermediate illumination strengths and voltages [9] regular relaxation oscillations of the total current were observed [Fig. 2(f)]. In parallel, the spatially averaged ellipsomicroscopic light intensity $\langle R \rangle$ oscillates sinusoidally and is phase-locked to the current oscillations [Fig. 2(e)]. In contrast to the regular time series of the averaged quantities, snapshots of the electrode [Figs. 2(a) and 2(b)] reveal that the oxide layer thickness forms an intricate and time-dependent labyrinthine pattern. The two images are taken at two successive maxima of the average oxide layer thickness. As most easily seen in the encircled areas, in successive oscillations the bright and dark regions exchange their positions, suggesting that the overall dynamics is not simple periodic with the period of the total current. More insight into the spatiotemporal dynamics is obtained when looking at the temporal evolution along the 1D cut shown in Fig. 2(c). In this representation, one obtains the impression that a uniform oscillation with the base frequency is superimposed on an irregular pattern that changes in time. The characteristics of the dynamics become apparent when looking at the level of the local time series [Fig. 2(d)]. The local oscillation amplitude evolves irregularly in time and is different for each oscillator shown. However, the extrema of R for all individual oscillators are locked to the ones of the average signal $\langle R \rangle$ (a few extrema disappear due to a large modulation of the local oscillation). The envelope of the complex dynamics of each individual oscillator contains harmonic contributions with half the base frequency (i.e., the one of the homogeneous oscillation). This is clearly seen when performing a Fourier transform of the time series $R(t)$ of each

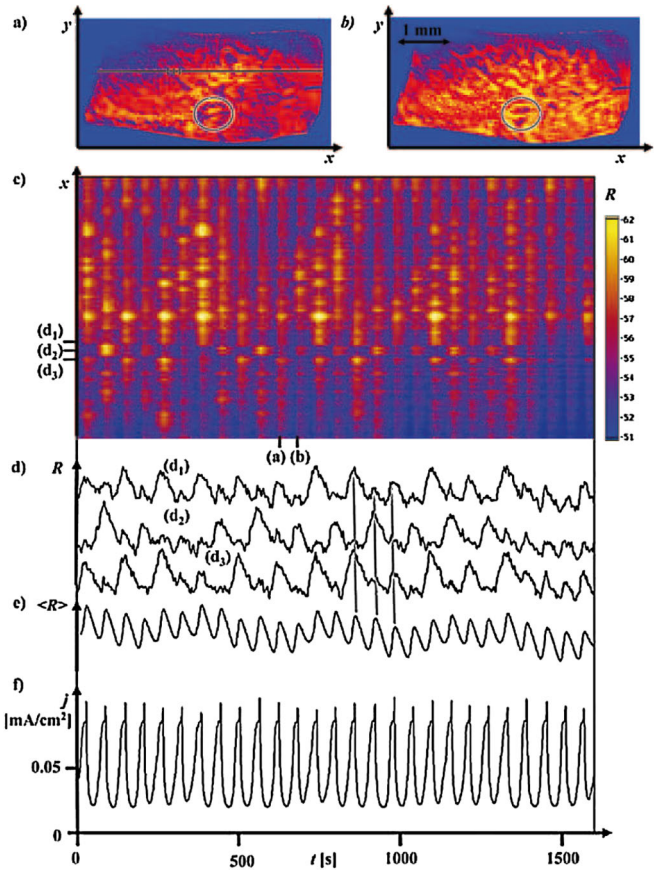

FIG. 2 (color online). Spatiotemporal data during n-Si electrodissolution at a voltage $U = 11.65$ V. (a),(b) Ellipsomicroscopic snapshots of the Si electrode taken at subsequent maxima of the average light intensity $\langle R \rangle$. (c) Spatiotemporal evolution of $R(x, t)$ for the 1D cut indicated in (a). (d) Local time series of $R(t)$ for the three points indicated in (c). (e) Time evolution of $\langle R \rangle$. (f) Time evolution of the total current.

local oscillator. In Fig. 3(a) the amplitude of the Fourier transform a is displayed for the data of Fig. 2(c) as a function of frequency. Two main peaks are observed for all time series: the one at the base frequency (17 mHz), a_1, and a subharmonic one at half the base frequency (8.5 mHz), $a_{1/2}$. To get an understanding of the 2D spatial distribution of these modes, we use a frequency demodulation technique [10]. In Fig. 3(b), the spatial distribution $|a_1|$ of the amplitude of the mode at the base frequency is shown. The amplitude for this mode is homogeneously distributed, all oscillators being also clustered to the same phase, as can be seen in Fig. 3(d). This is evident also from Figs. 3(f) and 3(g), where the phase histogram and the distribution of a_1 in the complex plane are given, respectively. The behavior of this mode is related to the locking of the amplitude extrema of all individual oscillators to the average signal. The subharmonic Fourier mode $a_{1/2}$ is shown in Figs. 3(c) (amplitude) and 3(e) (phase). Two domains having the same amplitude but opposite phase are entangled in a labyrinthine pattern.

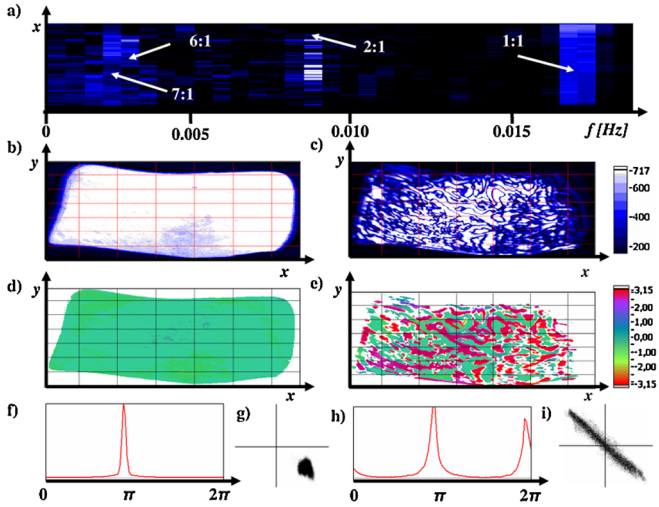

FIG. 3 (color online). Fourier transform of the data shown in Fig. 2 and amplitude and phase distributions of the coefficients of the main frequencies. (a) Amplitude of the Fourier transform a of the local time series of R along the 1D cut in Fig. 2(c). (b), (c) 2D distribution of the amplitude of the main Fourier mode $a_1(x, y)$ and of the subharmonic mode $a_{1/2}(x, y)$, respectively. (d),(e) 2D distribution of the phase of the main Fourier mode $a_1(x, y)$ and of the subharmonic mode $a_{1/2}(x, y)$, respectively. (f),(h) Phase histogram for all spatial points of a_1 and $a_{1/2}$, respectively. (g),(i) Representation in the complex plane of a_1 and $a_{1/2}$, respectively.

From the phase histogram Fig. 3(h) and the representation of $a_{1/2}$ in the complex plane Fig. 3(i), we see that 2-phase clustering occurs, with Ising walls (i.e., boundaries where $|a_{1/2}| = 0$) separating the clustered domains where the phase abruptly changes by π radians. These 2-phase clusters are phase balanced; i.e., there is the same amount of oscillators in each phase.

The illumination strength limits the number of electron-hole pairs available for the oxidation of Si and introduces a constraint on the maximum total current. Making the plausible assumption that electrical quantities, such as the concentration of holes at the surface, always remain uniformly distributed but oscillate in time, these self-induced oscillations could act like a harmonic forcing. On the other hand, it is known that an external resistor introduces a global coupling [2]. Thus, there are two global sources that affect the dynamics. The local oscillators are entrained to the base mode leading to locking of the amplitude extrema. A theoretical model to describe the main observations above is provided by a modified complex Ginzburg-Landau equation

$$\partial_t W = W + (1 + ic_1)\partial_x^2 W - (1 + ic_2)|W|^2 W + B, \quad (1)$$

where

$$B = \gamma - (1 + i\nu)\langle W\rangle + (1 + ic_2)\langle |W|^2 W\rangle. \quad (2)$$

W is a complex amplitude and $\langle \cdots \rangle$ denotes spatial averages. The real part of the complex amplitude, $W_r \equiv \mathrm{Re}W$, describes the dynamics of the interfacial oxide thickness. Since the experimentally observed behavior in two dimensions possesses the same essential features as in the one dimensional cuts, we consider for simplicity a 1D model, with x denoting the spatial direction along one cut of the 2D sample. The first term in Eq. (2) describes a parametric forcing close to a 1:1 resonance [11]. The second and third terms describe the nonlinear effect of the global signal $\langle W\rangle$ on the dynamics of the system and can be thought of as an expansion of a negative global coupling to third order. The introduction of such global dynamics, with cubic terms on the spatial average of the amplitude, is motivated by analogous studies on phase ordering under a global conservation law [12]. While $\langle W\rangle$ is constant in [12] (the *real* Ginzburg-Landau equation is employed therein), in our case it is a periodically oscillating function as observed in our experiments [see Figs. 2(e) and 2(f)]. Consequently, $\langle W\rangle$ needs to be a periodic function in the most general description to reflect this constraint, and so it is in Eq. (1). This can be seen by taking spatial averages on both sides of Eq. (1): We obtain the differential equation $\partial_t\langle W\rangle = \gamma - i\nu\langle W\rangle$ which has the closed analytical oscillating solution $\langle W\rangle = i\gamma[\exp(-i\nu t) - 1]/\nu + \langle W\rangle_0 \exp(-i\nu t)$ where $\langle W\rangle_0$ is the initial spatial average. From this solution we observe that ν specifies the frequency of the homogeneous oscillation. It is to be noted that neither the parametric-force-like term nor the global-feedback-like ones in Eq. (1) correspond to an experimental time-dependent manipulation of the system but arise *intrinsically* from its dynamics; i.e., these terms are *self-induced* in the system.

We have carried out simulations with Eq. (1) by using a pseudospectral method with 1000 Fourier modes, no flux boundary conditions and uniform noise superimposed on a localized pulse as initial condition. The integration is carried out by means of an exponential time stepping algorithm [13]. The spatiotemporal evolution of the real part of the complex amplitude W_r is shown in Fig. 4(a). We observe an irregular pattern like in the experiment [Fig. 2(c)]. Further analysis also reveals a high degree of organization. In Fig. 4(b) we see, for example, that any individual oscillator has complicated modulations in the amplitude that render the spatial pattern irregular. Yet all extrema are locked to the ones of the average signal $\langle W_r\rangle = \mathrm{Re}\langle W\rangle$, possessing the same base periodicity. Also in the simulations, the spatial pattern is irregular because of complicated modulations in the amplitude from the subharmonic modes. This is also a most prominent feature in the experimental data [Figs. 2(d) and 2(e)]. The average signal slaves the individual oscillators although the modulation of the amplitude displays a complicated behavior. Performing a Fourier analysis of the simulated time series for each oscillator, we find two main peaks in the power spectrum as in Fig. 3(a), one at frequency ν and the other at the subharmonic $\nu/2$. This is the case for *all* local oscillators. In

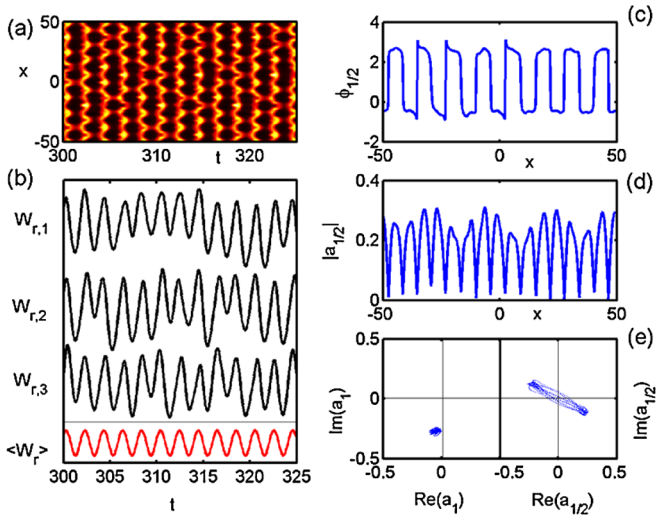

FIG. 4 (color online). (a) Spatiotemporal evolution of the real value W_r of the complex amplitude W obtained from Eq. (1) for $c_1 = -10$, $c_2 = 1.5$, $\gamma = 1.55$ and $\nu = 3.1$. (b) Local time series of $W_{r,i}$ for three individual oscillators i and time series of the spatial average $\langle W_r \rangle$. (c) 1D distribution of the phase of the first subharmonic Fourier mode $a_{1/2}$ of the time series at frequency $\nu/2$. (d) 1D distribution of the amplitude for the first subharmonic Fourier mode $a_{1/2}$ of the time series at frequency $\nu/2$. (e) Representation in the complex plane of $a_1(x)$ (left) and $a_{1/2}(x)$ (right).

Fig. 4(e) (left), it is shown that phase locking occurs at the base frequency ν for the base Fourier mode a_1 of the time series for all oscillators, which conforms with the observation made in Figs. 3(f) and 3(g). In Figs. 4(c) and 4(d), we plot the phase and amplitude, respectively, of the Fourier coefficient $a_{1/2}$ of the time series of W_r at the subharmonic frequency $\nu/2$ for all points in space. We see that clustering into two different phases occurs. The cluster domains are separated by Ising walls. The clustering is even more apparent in Fig. 4(e) (right), where $a_{1/2}$ is shown in the complex plane. Phase balance holds, with the same amount of oscillators in each phase [cf. Fig. 3(i)]. The simulations revealed that the nonlinear global coupling is responsible for all oscillators being locked at their extrema while the 1:1 resonance γ, which is intrinsic to the Si oxidation dynamics, contributes to the observed subharmonic 2-phase clustering.

In this Letter we have presented *in situ* measurements resolving the rich spatiotemporal dynamics at a semiconductor-electrolyte interface using ellipsomicroscopy. We have observed the formation of unusual subharmonic cluster patterns during the oscillatory electrooxidation of *n*-Si(111) whose properties have been elucidated by means of a modified complex Ginzburg-Landau equation.

We thank M. Dornhege and H. H. Rotermund for introducing us to ellipsomicroscopy and M. Frigieri, C. Fontanesi and A. Heinrich for help with experimental aspects. Financial support from the European Union (project DYNAMO, Contract No. 028669) and the cluster of excellence Nanosystems Initiative Munich (NIM) is gratefully acknowledged.

*Krischer@ph.tum.de

[1] Y. Kuramoto, *Chemical Oscillations, Waves and Turbulence* (Springer Series in Synergetics, Berlin, 1984).
[2] K. Krischer, in *Advances in Electrochemical Sciences and Engineering*, edited by D. M. Kolb and R. C. Alkire (Wiley-VCH, Weinheim, 2003), p. 89.
[3] P. Coullet *et al.*, Phys. Rev. Lett. **65**, 1352 (1990); P. Coullet and K. Emilsson, Physica (Amsterdam) **61D**, 119 (1992); C. Elphick, A. Hagberg, and E. Meron, Phys. Rev. Lett. **80**, 5007 (1998); M. Bertram, C. Beta, H. H. Rotermund, and G. Ertl, J. Phys. Chem. B **107**, 9610 (2003); P. Kaira *et al.*, Phys. Rev. E **77**, 046106 (2008); A. L. Lin, A. Hagberg, E. Meron, and H. L. Swinney, Phys. Rev. E **69**, 066217 (2004).
[4] M. Kim *et al.*, Science **292**, 1357 (2001); L. F. Yang, M. Dolnik, A. M. Zhabotinsky, and I. R. Epstein, Phys. Rev. E **62**, 6414 (2000); H. Varela, C. Beta, A. Bonnefont, and K. Krischer, Phys. Chem. Chem. Phys. **7**, 2429 (2005); V. Garcia-Morales and K. Krischer, Phys. Rev. E **78**, 057201 (2008); V. K. Vanag, A. M. Zhabotinsky, and I. R. Epstein, J. Phys. Chem. A **104**, 11 566 (2000).
[5] D. J. Blackwood *et al.*, Electrochim. Acta **37**, 889 (1992); D. R. Turner, J. Electrochem. Soc. **105**, 402 (1958); H. Gerischer and M. Lübke, Ber. Bunsenges. Phys. Chem. **92**, 573 (1988); E. Foca, J. Carstensen, and H. Foll, J. Electroanal. Chem. **603**, 175 (2007).
[6] M. Aggour, M. Giersig, and H. J. Lewerenz, J. Electroanal. Chem. **383**, 67 (1995); V. Lehmann, J. Electrochem. Soc. **143**, 1313 (1996); O. Nast, S. Rauscher, H. Jungblut, and H. J. Lewerenz, J. Electroanal. Chem. **442**, 169 (1998); F. Yahyaoui *et al.*, J. Electrochem. Soc. **149**, E472 (2002); J. Carstensen, R. Prange, G. S. Popkirov, and H. Foll, Appl. Phys. A **67**, 459 (1998); J. Stumper and L. M. Peter, J. Electroanal. Chem. **309**, 325 (1991).
[7] H. H. Rotermund *et al.*, Science **270**, 608 (1995); C. Punckt *et al.*, Science **305**, 1133 (2004).
[8] R. Memming and G. Schwandt, Surf. Sci. **4**, 109 (1966); M. Matsumura and S. R. Morrison, J. Electroanal. Chem. **144**, 113 (1983).
[9] S. Rauscher, Diploma thesis, Hahn Meitner Institut, Berlin, 1993.
[10] A. L. Lin *et al.*, Phys. Rev. Lett. **84**, 4240 (2000).
[11] J. Kim, J. Lee, and B. Kahng, Phys. Rev. E **65**, 046208 (2002).
[12] M. Conti, B. Meerson, A. Peleg, and P. V. Sasorov, Phys. Rev. E **65**, 046117 (2002).
[13] S. M. Cox and P. C. Matthews, J. Comput. Phys. **176**, 430 (2002).